PAPER

Bifunctional solid state electrochromic device using WO$_3$/WS$_2$ nanoflakes for charge storage and dual-band color modulation†

Suchita Kandpal,[a] Love Bansal,[a] Anjali Ghanghass,[b] Tanushree Ghosh,[a] Chanchal Rani,‡[a] Bhumika Sahu,[a] Deb Kumar Rath,[a] Ravi Bhatia,[b] I. Sameera ⓘ *[b] and Rajesh Kumar ⓘ *[ac]

A new methodology to enhance electrochromic performance and make it multifunctional ready has been demonstrated where an all-organic solid state electrochromic device has been made to display dual band color switching in the visible and near-infrared (NIR) spectrum. Additionally, energy storage capabilities have been added to make it a multifunctional solid-state device. A mixture of WS$_2$/WO$_3$ synthesized by the hydrothermal technique was characterized by X-ray diffraction, scanning electron microscopy (SEM), and Raman microscopy, prior to being used as a dopant with polythiophene (P3HT) and ethyl viologen (EV) active electrochromic layers. *In situ* kinematics was performed to check the electrochromic performance of the device in two wavelength (visible ~515 nm and NIR ~800 nm) regions. The fabricated device shows improved electrochromic performance in terms of switching time, color contrast, efficiency, and stability/cyclability in both wavelength regions of the electromagnetic spectrum. A very small external voltage bias (±1.5 V) was enough to switch the device (magenta ↔ blue) very quickly by taking less than a second's time. Furthermore, the supercapacitive performance parameters of the device have been investigated through cyclic voltammetry (CV), galvanostatic charge/discharge (GCD) curves, and electrochemical impedance spectroscopy (EIS). The results show that the specific capacitance value of the device is ~50 F g^{-1} at a current density of 1 A g^{-1} along with a fast response (charging/discharging) time and excellent energy density. The designed electrochromic supercapacitor device successfully demonstrated excellent capacitive performance along with ability as an electrochromic indicator and paves the way for the integration of electrochromic energy storage indicators in various energy storage or energy-efficient buildings.

1. Introduction

Smart electrochromic devices (ECDs),[1–4] which can control transmittance light through small applied voltages are becoming preferred choices for use in electrochromic smart windows/displays that can regulate the amount of light entering a building.[5] In addition to the inherent color changing

[a] *Materials and Device Laboratory, Department of Physics, Indian Institute of Technology Indore, Simrol-453552, India. E-mail: rajeshkumar@iiti.ac.in*

[b] *Department of Physics, Guru Jambheshwar University of Science & Technology, Hisar, 125001, India*

[c] *Centre for Advanced Electronics, Indian Institute of Technology Indore, Simrol-453552, India*

‡ Current address: Department of Chemistry, University of Michigan, Ann Arbor, Michigan 48109, United States of America.

applications, recently, the functionalities of these devices have been extended by adding energy storage technology, which is referred to as electrochromic supercapacitors (ESCs).[6–8] The research on dual-functioning electrochromic devices is increasing because these devices not only change their optical properties (color or transparency) but also store energy by the applied external voltage. Moreover, solar radiation transmittance can also be modulated by electrochromic windows to control the temperature of the ambience, which is very promising for designing energy efficient buildings.[9–12] This application is more helpful if the device displays color modulation in the infrared (IR) region, which actually is the major component that causes heating. In other words, an electrochromic device with dual band color switching and added supercapacitive capabilities will be a technologically advantageous device to demonstrate. Therefore, incorporating smart materials in devices is highly desirable for multiple applications that can easily allow estimating or determining the storage of electrical

energy, which is of great significance. Materials showing overlapping properties between electrochromic and supercapacitive nature may be a great choice to design such multifunctional devices.

It is well-known that the electrode material plays a vital role to achieve high-performance ESCs, which contain a series of active electrodes including metal oxides/dichalcogenides, carbon-based materials, MOFs, conducting polymers, and their composites.[13–23] Some transition metal oxides or conducting polymers such as polythiophene, polyaniline, WO_3, V_2O_5, MnO_2, *etc.* are widely used active materials for both electrochromic and energy storage applications due to their faradic reactions between the active material and electrolyte.[24,25] However, a large proportion of CPs have poor cycling stability, but polythiophene (P3HT)[26,27] is one of the most favorable materials in the field of electrochromic and energy storage due to its high conductivity, good thermal properties, and long-term stability. Though the value of its capacitance is not much, it can potentially be enhanced by doping with 2D materials, capable of offering a large surface area, more electroactive sites, and faster ion transport properties. Despite offering all these merits, the transition metal dichalcogenides (TMDs) still suffer from poor cycle life due to the restacking of the nanolayers. The poor structural integrity can be resolved by developing composites or mixtures, or developing hybrid core/shell nanostructures.[28–31] Among the TMDs, WS_2 with a covalently bonded S–W–S layered structure offers a large surface area, making it one of the ideal energy storage materials, but on the other side, its inherent color decreases the electrochromic color contrast.[32–35] Thus, nanoflakes of WS_2/WO_3 might be a good option to opt for as a dopant to make a device suitable for electrochromic as well as energy storage applications without compromising the electrochromic performance of the device. Using the WS_2/WO_3 combination as a dopant, in a device fabricated using well-established electrochromic materials, instead of the main active layer, could be a better choice as they will help in managing the redox activity without hindering the electrochromic operation as has been investigated here.

In the current work, a mixture of WS_2/WO_3 was synthesized, by a hydrothermal technique, for utilization in fabricating a multifunctional P3HT/EV-based electrochromic charge storage device. *In situ* bias-dependent UV-Vis spectroscopy and electrochemical measurements show a fast switching between magenta and blue states with a small bias of 1.5 V. Compared with the undoped polythiophene-based devices, the fabricated device has outstanding electrochromic/supercapacitor properties in terms of a large contrast ratio of ~52%, fast switching speeds (0.5 s/0.7 s at $\lambda \sim 515$ nm and 0.8 s/0.8 s at $\lambda \sim 800$ nm), excellent coloration efficiency and high specific capacitance along with charging/discharging stability under fast switching conditions. The successfully fabricated multifunctional solid-state device displays a change in color under small external bias and stores the energy supplied for coloration making it a multifunctional energy-storing ECSD with great potential for use in the next-generation smart electrochemical components. The multifunctional solid state ECD, in addition to the above-mentioned dual application in energy storage & electrochromic color change, displays color modulation in two bands *vis-e-vis* visible as well as near infrared. The latter may give an additional advantage in designing thermal control smart windows to be used in next-generation smart electrochemical components.

2. Experimental details

2.1 Chemicals used

Commercial grade chemicals, polyethylene oxide (PEO, Alfa Aesar, M_W = 100 000), ethyl viologen diperchlorate (EV, 98%, Sigma Aldrich), poly(3-hexyl thiophene-2,5-diyl) (P3HT, regioregular, Sigma Aldrich), ammonium paratungstate, thiourea, 1,2-dichlorobenzene (DCB, anhydrous, 99%, Sigma Aldrich) and acetonitrile (ACN, anhydrous, 99%, Sigma Aldrich) were used for device fabrication in the present study.

2.2 WS_2/WO_3 synthesis

A facile one-step hydrothermal method was used for the synthesis of WS_2/WO_3 nanoflakes. The synthesis was performed using 1:3 weight ratio of ammonium paratungstate $[(NH_4)_{10}(H_2W_{12}O_{42})\cdot 4H_2O]$ and thiourea $[(NH_2)_2CS]$. The precursors were dissolved in 70 mL of de-ionized water by continuous stirring for 30 minutes. A homogeneous and colorless solution was obtained after stirring. The solution was transferred into a 100 mL Teflon-lined stainless steel hydrothermal reactor. The reactor was heated to 240 °C in a muffle furnace for 3 h and then allowed to cool down to room temperature. The nanoflake sample in the form of a greyish black precipitate was collected after centrifugation and then washed with de-ionized water and ethanol several times. The reaction product was dried overnight using a vacuum oven at 60 °C.[36,37]

2.3 Device fabrication

For the fabrication of the electrochromic device (ECD), thin films of P3HT and WS_2/WO_3 doped ethyl viologen, grown through the spin coating and drop casting techniques over ITO-coated glass substrates, have been used. For this, three different solutions *i.e.*, 0.3 wt% P3HT in DCB, 5 wt% PEO in ACN and 4 wt% EV in ACN were prepared by using vortex mixing. The P3HT film (~1 μm thick) was spin-coated on an ITO-coated glass substrate at 500 rpm for 120 s and then annealed at 80 °C for one hour, whereas a layer of EV (premixed with WS_2/WO_3) in a PEO matrix was drop casted on another ITO coated glass substrate and then assembled together with the help of double-sided tape using the simple flip-chip method as reported elsewhere in detail.[38]

2.4 Characterization and measurements

Structural and morphological characterizations of the synthesized nanoflakes have been carried out by using a Rigaku Smart lab Multipurpose Versatile XRD and 7610F Plus/JEOL field emission scanning electron microscope (FESEM). Raman spectra were recorded at a wavelength of 532 nm by using an

This journal is © The Royal Society of Chemistry 2023

J. Mater. Chem. C, 2023, **11**, 12590–12598 | **12591**

Alpha300/WITec Raman spectrometer. Electrochemical measurements of the device have been done using a Keithley-2450 workstation and a Metrohm-Multi Autolab M204 potentiostat. The PerkinElmer make lambda 365 spectrometer was used for all *in situ* bias-dependent UV-Vis measurements.

3. Results and discussion

Prior to making an electrochromic energy storage device, hydrothermally synthesized WS_2/WO_3 nanoflakes have been characterized by SEM, XRD and Raman spectroscopy.

The FESEM micrograph (Fig. 1(a)) depicts the morphological aspect of the hydrothermally synthesized WS_2/WO_3 nanoflakes. It can be clearly observed that the synthesized nanoflakes have a thickness in the range of ~10 nm. The EDS measurements (Fig. S1, ESI†) reveal the presence of W, O and S in the sample, which confirms the nanoflakes of WS_2/WO_3. The structural characteristics were analyzed using XRD data (Fig. 1(b)). The diffraction peaks at ~ 13.7°, 28.7°, 31.3°, 39.0°, 43.0°, 49.47°, 59.3°, 65.4° and 75.8° correspond to the (002), (004), (101), (103), (006), (105), (112), (114) and (205) planes of the 2H-phase of WS_2 [JCPDS card no: 08-1398] and the peaks at 24.0°, 27.7°, 34.0°, 36.9°, 42.1°, 47.1°, 54.0° and 57.7° correspond to the (001), (200), (111), (201), (300), (002), (221) and (400) planes of the hexagonal phase of WO_3 [JCPDS card no: 75-2187].[39,40] The peak marked by an asterisk (*) represents the (111) plane of orthorhombic $WO_3 \cdot 0.33H_2O$.[41] The structural features of the nanoflake sample have been further verified using Raman spectroscopy (inset, Fig. 1(b)). The peaks centered at ~351.5 and 420.5 cm^{-1} are attributed to the E_{2g}^1 and A_{1g} modes of WS_2.[42] The E_{2g}^1 mode is associated with the interlayer atomic vibrations of the W–S bond with both the atoms moving in opposite directions, whereas the A_{1g} mode is related to the intralayer vibrations of S atoms. The peaks at ~173 and 269 cm^{-1} represent the bending (W–O–W) mode of the bridging oxygen, whereas the peak at ~788 cm^{-1} corresponds to the stretching (O–W–O) vibrational mode of tungsten atoms

and adjacent oxygen atoms of hexagonal WO_3.[42] An estimate of the thickness of the nanoflakes can be obtained by using the difference in the peak position of the E_{2g}^1 and A_{1g} modes of the Raman spectrum (Fig. 1(b), inset). The frequency difference between the modes is ~69 cm^{-1}, which represents ~3–4 layer thick WS_2/WO_3.[43,44]

As planned, the above-characterized nanoflakes of WS_2/WO_3 have been used as a dopant to make a multifunctional solid-state ECD by following the recipe mentioned in the experimental section. The ECD having structure "ITO glass/P3HT/(WO_3/WS_2 + EV)/ITO" glass was obtained by sandwiching the P3HT and EV (doped with WO_3/WS_2) in PEO gel electrodes, as shown in the schematic (Fig. 2(a)). The finally prepared device appears in its magenta color due to the inherent color of pristine P3HT with the EV layer being transparent. As the external power supply (+1.5 V, with respect to P3HT) is applied across the two different electrodes of the device, the device changes its initial magenta color to blue color as shown in the actual photographs of the device (inset, Fig. 2(a)). This is because of the reduction of the EV^{2+} ion to its $EV^{\bullet+}$ radical cation and comes from its transparent state to a blue state.[45] Subsequently, neutral P3HT gets oxidized by losing its electron to the electrode and changes its magenta color to its transparent color through a dynamic doping process. Thus, the simultaneous change in the color of both electrodes gives the overall blue color to the device, which can also be understood using the bias-dependent UV-Vis transmission spectra of the device as has been discussed later on. On reversing the bias polarity (−1.5 V), the device comes back to its magenta color (Fig. 2(b)) due to the bias reversal redox behavior of both the EV and P3HT electrodes.

The color change of the device can also be understood by the bias-dependent transmission spectra of the device (Fig. 2(b) and (c)), which shows the change in optical transmittance of the device as a function of applied bias and can be correlated with the perceived color of the device. The maximum transmission occurs in the blue and red wavelength regions of the

Fig. 1 (a) FESEM micrograph; (b) XRD pattern of WS_2/WO_3 nanoflakes along with their Raman spectra (inset).

12592 | *J. Mater. Chem. C*, 2023, **11**, 12590–12598

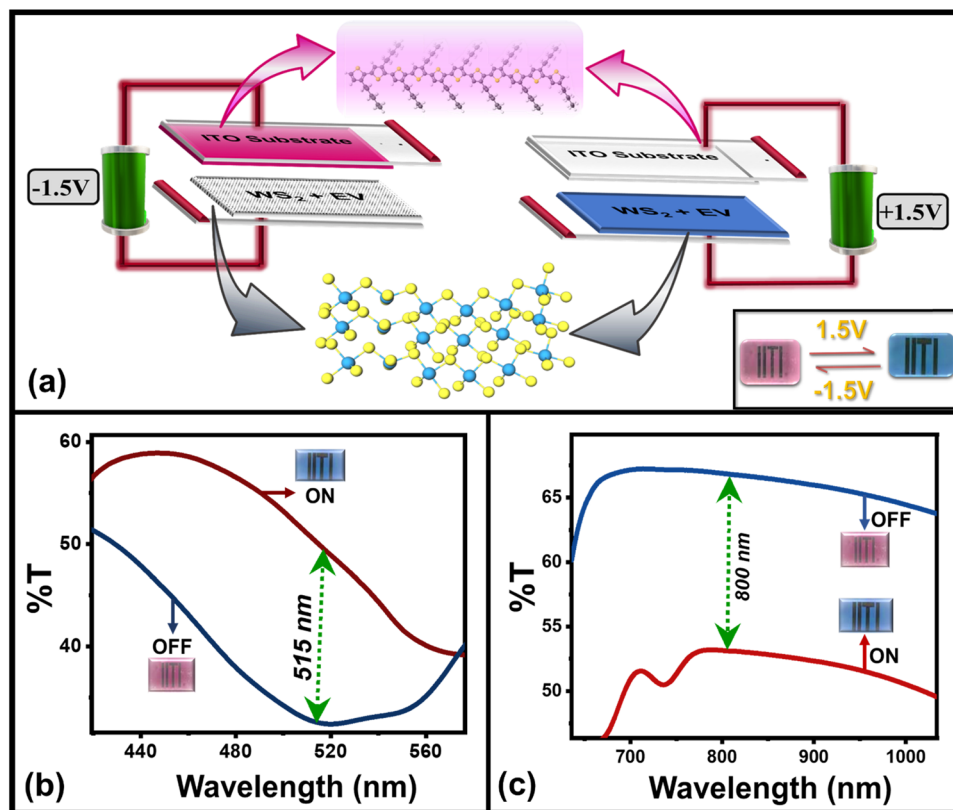This journal is © The Royal Society of Chemistry 2023

Fig. 2 (a) Schematic representation of the layered device along with its actual photographs (inset) under different bias conditions, (b) *in situ* bias dependent transmission spectra of the device in the visible (∼515 nm) as well as NIR (∼800 nm) wavelength region in (c). Graphics Partly adopted with permission from ref. 26 Copyright American Chemical Society (2023).

visible spectrum, which gives the initial (magenta, OFF) color to the device (blue curve, Fig. 2(b)) whereas the colored (blue or "ON") state is characterized by the overall transmission band in the lower energy (blue wavelength) region (red curve, Fig. 2(b)) and giving the blue appearance to the device. There is an increased transmission of IR-radiation in the OFF state of the device whereas suppressed transmission in the IR-radiation value, as a function of applied bias. It can be appreciated from Fig. 2(c), which shows the multiwavelength transmission modulation of the device in the visible (∼515 nm) as well as NIR (∼800 nm) wavelength regions. The device has sufficiently good color contrast in the visible wavelength region with a maximum value of ∼52% at 515 nm. The device shows reversible color switching between the two colors represented through the CIE color coordinates (u',v') of (0.381, 0.362) in the OFF state and (0.198, 0.262) in the ON state, as shown in Fig. 3. It also maintains its good contrast value corresponding to a higher wavelength in the near infrared (NIR) region. Therefore, these two wavelength regions have been chosen to carry out investigations related to the electrochromic switching behavior of the device by measuring its switching kinetics.

In addition to the color contrast of the device, switching stability/cyclability is another important parameter, when we examine the electrochromic performance of an electrochromic
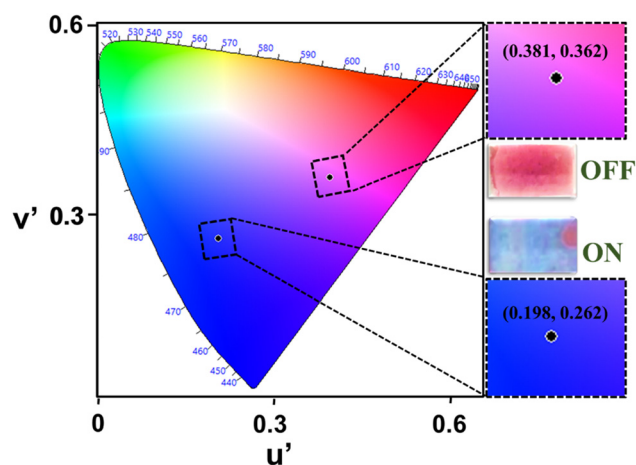

Fig. 3 Color identification through the CIE chart of the fabricated device and the corresponding images.

device (Fig. 4). The device shows excellent switching stability of at least 1000 seconds when the device is continuously toggled between ON/OFF states with an applied square pulse of ±1.5 V amplitude of 5 s time intervals each at 515 nm and 800 nm wavelength regions, respectively. The ECD exhibited less variation in absorbance even after the 200 repeated operation cycles
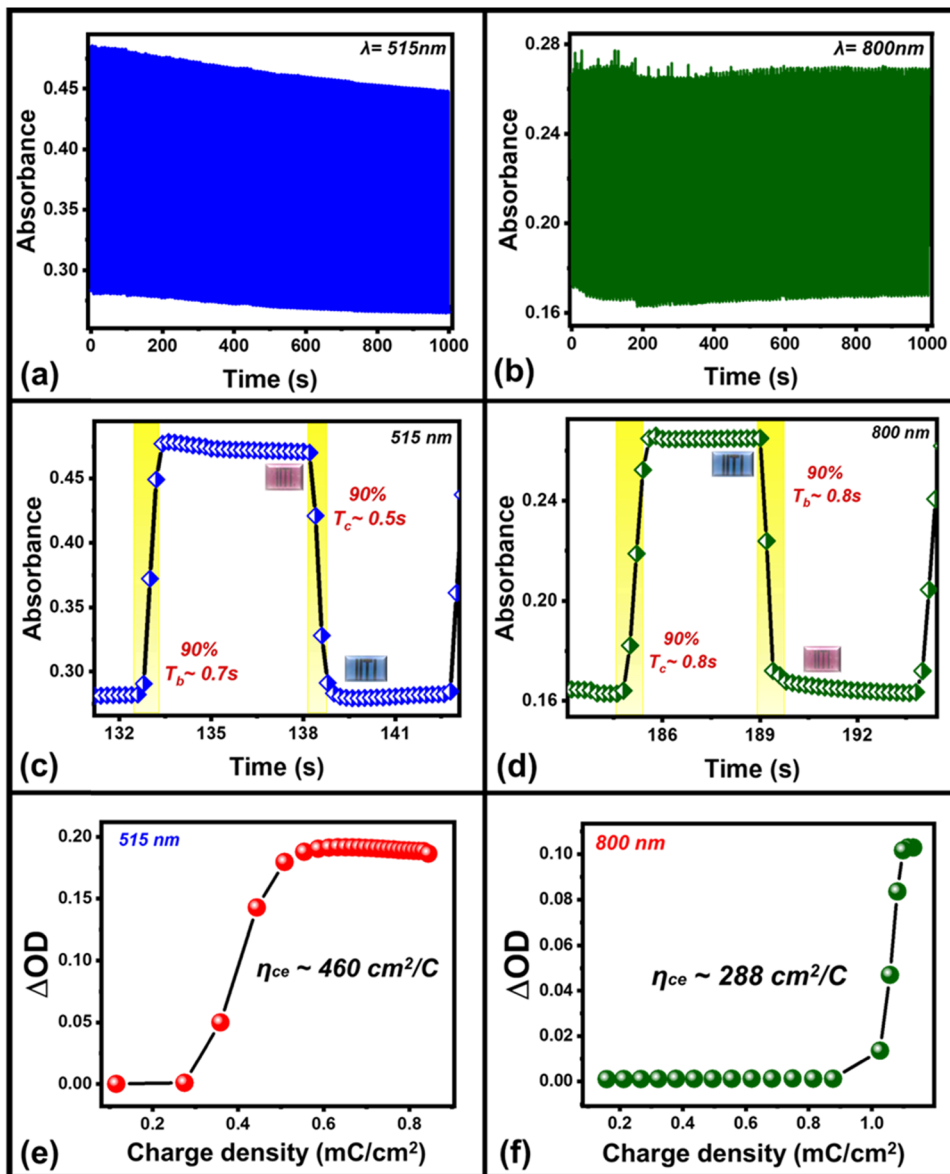
This journal is © The Royal Society of Chemistry 2023

J. Mater. Chem. C, 2023, **11**, 12590–12598 | **12593**

Fig. 4 (a) *In situ* bias-dependent multiple switching cycles of the device between ON and OFF states in the voltage window (±1.5 V) in the visible and infrared (IR) wavelength region in (b) and (c) single switching cycle at 515 nm wavelength, (d) response time of the device in the same fixed voltage window at 800 nm wavelength, and the corresponding estimated coloration efficiencies of the device in (e) and (f).

in the visible ($\sim$515 nm, Fig. 4(a)) wavelength region whereas the repeated switching cycles in the infrared (IR) ($\sim$800 nm) region show some spikes in the absorbance values due to the external environmental disturbance while recording the repeating switching cycles of the device (Fig. 4(b)). The significantly lower variation in absorbance in the repetition of such switching steps up to 1000 s or 200 switching cycles shows a great stability/cyclability of the device in both wavelength regions.

One of these absorbance switching cycles has been used to measure the switching time taken by the device to toggle between its ON and OFF states (Fig. 4(c) and (d)). The switching time is defined as the time taken by the device to show 90% change in the absorbance value. The as-prepared device takes 500 ms to switch from its OFF state (magenta) to ON state

(blue), while 700 ms is required to switch back to the OFF state from the ON state in the visible ($\sim$515 nm) wavelength region (Fig. 4(c)) whereas its switching time in the IR-wavelength ($\sim$800 nm) region is 0.8 s (coloration, ON)/0.8 s (bleaching, OFF), respectively (Fig. 4(d)). A switching time of less than a second shown by the device represents a fast switching that has been achieved due to the presence of the mixture of WS_2/WO_3 as it can store charge carriers under external bias, which facilitates the necessary charges to take part in reversible redox reaction to P3HT in ECD that can be compared with the device in the absence of the mixture of WS_2/WO_3 (Fig. S2, ESI†). Additionally, the coloration efficiency (CE)[46,47] is one of the most crucial parameters to measure the performance of an ECD in terms of the overall power efficiency, which is estimated by

the formula given in eqn (1) below:

$$\eta_{ce} = \frac{\Delta OD(\lambda)}{Q}, \quad (1)$$

where η_{ce} is the CE in $cm^2\ C^{-1}$, ΔOD is the variation in optical density which is defined as $A_f - A_n$, with A_f and A_n being the absorbance values of the device in its OFF and ON states, and Q ($C\ cm^{-2}$) is the charge density required to display the above difference in the OD. Herein, the coloration efficiency of the device was calculated from the slope of the curve plotted between the change in optical density (ΔOD) and the charge density (Q) obtained from Fig. 4(e), (f) and comes out to be 460 $cm^2\ C^{-1}$ and 288 $cm^2\ C^{-1}$ for visible (~ 515 nm) and infrared (IR) (~ 800 nm) wavelength regions, respectively. These values of a few hundreds represent moderately high coloration efficiency from a device in its solid-state form making it a good option for power efficient operation. The better performance of the device is also evident from the comparison table below (Table 1). As mentioned above, the possible reason for the improved color switching performance is the charge storage capability of WS_2/WO_3, which gives the device a possibility to be explored for charge storage applications as has been discussed below.

The (super-)capacitive property of the electrochromic device has also been optimized through cyclic voltammetry (CV), electrochemical impedance spectroscopy (EIS), and galvanostatic charge–discharge (GCD) curves. The CV curves of the fabricated solid-state ECD at different scan rates from 100 mV s^{-1} to 400 mV s^{-1} with the potential range of -1.5 V to 2 V have been recorded (Fig. 5(a)) which shows a pair of redox peaks indicating pseudocapacitive behavior of WS_2/WO_3 nanoflakes. Furthermore, the movement of ion diffusion in an electrochromic device has been investigated by EIS using a Nyquist plot (Fig. 5(b)) up to the frequency range of 100 kHz to 10 mHz. The Nyquist plot exhibits a semicircle and linear regiment representing high- and low-frequency regions, respectively. The semi-circle in the high-frequency region is associated with the contact resistance between the solution and electrolyte whereas the linear regiment at the low-frequency region associated with the redox mechanism occurs at the electrode–electrolyte interface, which indicates the capacitive behavior of the fabricated hybrid electrochromic device. To fit the EIS analysis data, an equivalent electrical circuit (inset, Fig. 5(b)) has been plotted, which shows the small charge

transfer resistance, indicating fast charging and discharging response time of the device.

Furthermore, the electrochemical performance of the device has been investigated through the galvanostatic charge/discharge curve with different current densities (1 A g^{-1} to 2 A g^{-1}) using a potential window from 1.6 V to -1.6 V. The deviation from the ideal triangular shape of the GCD curves indicates the contribution from the pseudocapacitive charge storage behavior of the device. The small infrared (IR) drop present in the GCD curves of the device also shows the small charge transfer resistance offered by the electrolyte ions as also expected from the EIS plot. It is also clearly seen that the discharging time decreases with the increase in the current density due to the faster diffusion of electrolyte ions on the active material of the device. A bit longer discharging time, than charging time, indicates the high Coulombic efficiency of the device, which makes it suitable for practical applications. This can also be seen in the recorded time dependent absorbance spectrum curve (Fig. S3, ESI†) of the device during charging and discharging, which also shows the decreasing absorbance value during the discharging process, which is one of the crucial factors for electrochromic supercapacitors. Furthermore, the specific capacitance[51,52] of the device has been calculated from a GCD plot using the equation (eqn (2)) mentioned below:

$$C_s = \frac{I \Delta t}{m \Delta V}, \quad (2)$$

where, I is the discharge current, Δt is the discharge time, ΔV is the potential window and m is the active material mass over the electrode. The obtained maximum specific capacitance value for the device is ~ 50 F g^{-1} at a current density of 1 A g^{-1} and shows a typical variation with current density, as shown in Fig. 5(d). A gradual decrease in specific capacitance with current density also indicates the pseudocapacitive nature of the device. Since high energy density is desired and is one of the factors which makes supercapacitor devices suitable for practical applications, the energy density[53,54] of the device has been calculated using eqn (3) mentioned below:

$$E_D = \frac{1}{2} C_s (\Delta V)^2, \quad (3)$$

where C_s is the calculated specific capacitance of the device and ΔV is the working potential window. The maximum energy density of the device is calculated to be ~ 60 W h kg^{-1} (inset, Fig. 5(d)) at a current density of 1 A g^{-1}.

Based on the above discussion, it is very clearly evident that a solid-state electrochromic device *vis-e-vis* ITO/(EV + WS_2/WO_3)/P3HT/ITO shows not only an improvement in electrochromic performance but also displays moderately high super capacitive performance. The two properties, namely improved electrochromic performance and charge storage capabilities, are complementary to each other and support mutual operation. Incorporation of WS_2/WO_3 plays a key role by storing charge to facilitate the necessary redox process in a better way as well as thus assisting in necessary charge transport during

Table 1 Comparison table of various reported P3HT-based solid state electrochromic devices

S. no	Device composition	Switching time (s)	Coloration efficiency ($cm^2\ C^{-1}$)	Ref.
1	P3HT-NTTO	0.8	1055	Bansal *et al.*[26]
2	PANI/P3HT	0.5	534	Pathak *et al.*[48]
3	P3HT/PCBM	0.5	320	Chaudhary *et al.*[49]
4	P3HT/IAI/PET	0.3	252	Kim *et al.*[50]
5	P3HT/viologen	1.5	200	Chaudhary *et al.*[38]
6	P3HT/WO_3 + WS_2 + EV	0.5	460	This work

This journal is © The Royal Society of Chemistry 2023

J. Mater. Chem. C, 2023, **11**, 12590–12598 | **12595**

Fig. 5 (a) Cyclic voltammetry of the device for different scan rates, (b) Nyquist plot (inset: equivalent electric circuit), (c) charging/discharging curves with increasing current densities and (d) varying specific capacitance value along with the energy density variation of the device in the inset.

color switching of the device. This yields a better way to make an improved multifunctional solid state electrochromic device made using complementing redox active layers. In other words, the WS_2/WO_3 doping enables one to achieve (i) improved dual band electrochromic modulation in the visible and NIR range and (ii) multifunctional operation by adding charge storage making it an overall multifunctional electrochromic solid state device.

4. Conclusion

A multifunctioning all-organic solid-state electrochromic device with supercapacitance charge storage capabilities can be fabricated using WS_2/WO_3 nanoflakes. The well characterized WS_2/WO_3 nanoflakes when doped with the organic electrochromic materials, P3HT and EV, display power efficient multifunctional applications with a color switching between magenta and blue colors with a small bias of ± 1.5 V. The device shows a great contrast ratio of 52%, fast switching time of less than one second and excellent coloration efficiencies of 460 cm^2 C^{-1} and 288 cm^2 C^{-1} at wavelengths ~ 515 nm (visible), and ~ 800 nm (NIR), respectively. Additionally, the device exhibited a maximum capacitance of ~ 50 F g^{-1} and an energy density of ~ 60 W h kg^{-1} at a current density of 1 A g^{-1}. Furthermore, the GCD curves of the device show excellent response time and high coulombic efficiency with the increase

in current density, making it suitable for practical applications. The improved electrochromic super capacitive device originates from the mutually supporting redox behavior of the P3HT, EV, and charge-facilitating nature of WS_2/WO_3. The WS_2/WO_3 doping in an all-organic material combines two applications, namely improved dual band electrochromic modulation in the visible and NIR range and charge storage, making it an overall multifunctional electrochromic solid-state device where the latter itself shows switching in the dual color band.

Data availability statement

The data that supports the findings of this study are available within the article and ESI.†

Conflicts of interest

There are no conflicts to declare.

Acknowledgements

12596 | *J. Mater. Chem. C*, 2023, **11**, 12590–12598

This journal is © The Royal Society of Chemistry 2023

References

1 R. Kumar, R. G. Pillai, N. Pekas, Y. Wu and R. L. McCreery, *J. Am. Chem. Soc.*, 2012, **134**, 14869–14876.

2 Y. Alesanco, A. Viñuales, J. Palenzuela, I. Odriozola, G. Cabañero, J. Rodriguez and R. Tena-Zaera, *ACS Appl. Mater. Interfaces*, 2016, **8**, 14795–14801.

3 T. Ghosh, S. Kandpal, C. Rani, A. Chaudhary and R. Kumar, *Adv. Opt. Mater.*, 2023, **11**, 2203126.

4 A.-L. Alexe-Ionescu, A. Th Ionescu, N. Scaramuzza, G. Strangi, C. Versace, G. Barbero and R. Bartolino, *Phys. Rev. E: Stat., Nonlinear, Soft Matter Phys.*, 2001, **64**, 011708.

5 F. G. K. Baucke, K. Bange and T. Gambke, *Displays*, 1988, **9**, 179–187.

6 X. Chen, H. Lin, J. Deng, Y. Zhang, X. Sun, P. Chen, X. Fang, Z. Zhang, G. Guan and H. Peng, *Adv. Mater.*, 2014, **26**, 8126–8132.

7 S. Kandpal, T. Ghosh, C. Rani, A. Chaudhary, J. Park, P. S. Lee and R. Kumar, *ACS Energy Lett.*, 2023, **8**, 1870–1886.

8 Y. Guo, W. Li, H. Yu, D. F. Perepichka and H. Meng, *Adv. Energy Mater.*, 2017, **7**, 1601623.

9 T. S. Hernandez, C. J. Barile, M. T. Strand, T. E. Dayrit, D. J. Slotcavage and M. D. McGehee, *ACS Energy Lett.*, 2018, **3**, 104–111.

10 X. Guo, J. Chen, A. L.-S. Eh, W. C. Poh, F. Jiang, F. Jiang, J. Chen and P. S. Lee, *ACS Appl. Mater. Interfaces*, 2022, **14**, 20237–20246.

11 A. Chaudhary, D. K. Pathak, M. Tanwar, J. Koch, H. Pfnür and R. Kumar, *J. Mater. Chem. C*, 2020, **8**, 1773–1780.

12 H. J. Lee, C. Lee, J. Song, Y. J. Yun, Y. Jun and C. S. Ah, *J. Mater. Chem. C*, 2020, **8**, 8747–8754.

13 A. S. Shaplov, D. O. Ponkratov, P.-H. Aubert, E. I. Lozinskaya, C. Plesse, F. Vidal and Y. S. Vygodskii, *Chem. Commun.*, 2014, **50**, 3191–3193.

14 S. Y. Kim, T. Y. Yun, K. S. Yu and H. C. Moon, *ACS Appl. Mater. Interfaces*, 2020, **12**, 51978–51986.

15 X. Xia, Y. Zhang, D. Chao, C. Guan, Y. Zhang, L. Li, X. Ge, I. Mínguez Bacho, J. Tu and H. Jin Fan, *Nanoscale*, 2014, **6**, 5008–5048.

16 S. Kandpal, T. Ghosh, C. Rani, M. Tanwar, M. Sharma, S. Rani, D. K. Pathak, R. Bhatia, I. Sameera, J. Jayabalan and R. Kumar, *ACS Mater. Au*, 2022, **2**, 293–300.

17 S. Li, Y. Wang, J.-G. Wu, L. Guo, M. Ye, Y.-H. Shao, R. Wang, C. Zhao and A. Wei, *RSC Adv.*, 2016, **6**, 72037–72043.

18 A. Chaudhary, D. K. Pathak, T. Ghosh, S. Kandpal, M. Tanwar, C. Rani and R. Kumar, *ACS Appl. Electron. Mater.*, 2020, **2**, 1768–1773.

19 S. Kandpal, T. Ghosh, M. Sharma, D. K. Pathak, M. Tanwar, C. Rani, R. Bhatia, I. Sameera, A. Chaudhary and R. Kumar, *Appl. Phys. Lett.*, 2021, **118**, 153301.

20 T. Ghosh, S. Kandpal, C. Rani, L. Bansal, M. Tanwar and R. Kumar, *Adv. Electron. Mater.*, 2023, **9**, 2201042.

21 C. Liu, Y. Bai, W. Li, F. Yang, G. Zhang and H. Pang, *Angew. Chem., Int. Ed.*, 2022, **61**, e202116282.

22 J.-L. Yang, J.-M. Cao, X.-X. Zhao, K.-Y. Zhang, S.-H. Zheng, Z.-Y. Gu and X.-L. Wu, *EnergyChem*, 2022, **4**, 100092.

23 P. Geng, L. Wang, M. Du, Y. Bai, W. Li, Y. Liu, S. Chen, P. Braunstein, Q. Xu and H. Pang, *Adv. Mater.*, 2022, **34**, 2107836.

24 G. Cai, J. Wang and P. S. Lee, *Acc. Chem. Res.*, 2016, **49**, 1469–1476.

25 W. Guo, Z. Cong, Z. H. Guo, P. Zhang, Y. Chen, W. Hu, Z. L. Wang and X. Pu, *Adv. Funct. Mater.*, 2021, **31**, 2104348.

26 L. Bansal, T. Ghosh, S. Kandpal, C. Rani, M. Tanwar and R. Kumar, *ACS Appl. Eng. Mater.*, 2023, **1**, 577–583.

27 L. Groenendaal, F. Jonas, D. Freitag, H. Pielartzik and J. R. Reynolds, *Adv. Mater.*, 2000, **12**, 481–494.

28 B.-R. Huang, T.-C. Lin and Y.-M. Liu, *Sol. Energy Mater. Sol. Cells*, 2015, **133**, 32–38.

29 K. Ahmad, M. A. Shinde, G. Song and H. Kim, *Ceram. Int.*, 2021, **47**, 34297–34306.

30 K.-W. Kim, T. Y. Yun, S.-H. You, X. Tang, J. Lee, Y. Seo, Y.-T. Kim, S. H. Kim, H. C. Moon and J. K. Kim, *NPG Asia Mater.*, 2020, **12**, 1–10.

31 C. C. Mayorga-Martinez, A. Ambrosi, A. Y. S. Eng, Z. Sofer and M. Pumera, *Electrochem. Commun.*, 2015, **56**, 24–28.

32 A. Azam, J. Kim, J. Park, T. G. Novak, A. P. Tiwari, S. H. Song, B. Kim and S. Jeon, *Nano Lett.*, 2018, **18**, 5646–5651.

33 K. S. Kumar, N. Choudhary, D. Pandey, L. Hurtado, H.-S. Chung, L. Tetard, Y. Jung and J. Thomas, *Nanotechnology*, 2020, **31**, 435405.

34 V. V. Mohan, M. Manuraj, P. M. Anjana and R. B. Rakhi, *Energy Technol.*, 2022, **10**, 2100976.

35 Y. Wang, D. Kong, W. Shi, B. Liu, G. J. Sim, Q. Ge and H. Y. Yang, *Adv. Energy Mater.*, 2016, **6**, 1601057.

36 Q. Liu, X. Li, Z. Xiao, Y. Zhou, H. Chen, A. Khalil, T. Xiang, J. Xu, W. Chu, X. Wu, J. Yang, C. Wang, Y. Xiong, C. Jin, P. M. Ajayan and L. Song, *Adv. Mater.*, 2015, **27**, 4837–4844.

37 L. Wang, K. Wang, R. Huang, Z. Qin, Y. Su and S. Tong, *Chemosphere*, 2020, **252**, 126578.

38 A. Chaudhary, D. K. Pathak, S. Mishra, P. Yogi, P. R. Sagdeo and R. Kumar, *Sol. Energy Mater. Sol. Cells*, 2018, **188**, 249–254.

39 S. V. P. Vattikuti, C. Byon and V. Chitturi, *Superlattices Microstruct.*, 2016, **94**, 39–50.

40 I. Sharma, M. M. Ghangrekar, R. C. Biswal and K. Biswas, *J. Electrochem. Soc.*, 2015, **163**, F183.

This journal is © The Royal Society of Chemistry 2023

J. Mater. Chem. C, 2023, **11**, 12590–12598 | **12597**

41 Y. Li, Z. Tang, J. Zhang and Z. Zhang, *Appl. Catal., B*, 2017, **207**, 207–217.

42 V. N. Tuan, H. H. Do, T. Mahider, V. L. Quyet, N. T. Phan, S. H. Hong, J. H. Cho, V. D. Dung, S. H. Ahn and K. S. Young, *Nano Convergence*, 2021, **8**, 28.

43 H. Zeng, G.-B. Liu, J. Dai, Y. Yan, B. Zhu, R. He, L. Xie, S. Xu, X. Chen, W. Yao and X. Cui, *Sci. Rep.*, 2013, **3**, 1608.

44 L. Yuan and L. Huang, *Nanoscale*, 2015, **7**, 7402–7408.

45 S. Mishra, H. Pandey, P. Yogi, S. K. Saxena, S. Roy, P. R. Sagdeo and R. Kumar, *Opt. Mater.*, 2017, **66**, 65–71.

46 S.-H. Lee, H. M. Cheong, C. E. Tracy, A. Mascarenhas, A. W. Czanderna and S. K. Deb, *Appl. Phys. Lett.*, 1999, **75**, 1541–1543.

47 S. Kandpal, T. Ghosh, C. Rani, S. Rani, D. K. Pathak, M. Tanwar, R. Bhatia, I. Sameera and R. Kumar, *Sol. Energy Mater. Sol. Cells*, 2022, **236**, 111502.

48 D. K. Pathak, T. Ghosh, S. Kandpal, C. Rani and R. Kumar, *Opt. Mater.*, 2023, **137**, 113519.

49 A. Chaudhary, D. K. Pathak, M. Tanwar, P. Yogi, P. R. Sagdeo and R. Kumar, *ACS Appl. Electron. Mater.*, 2019, **1**, 58–63.

50 T.-H. Kim, S.-H. Park, D.-H. Kim, Y.-C. Nah and H.-K. Kim, *Sol. Energy Mater. Sol. Cells*, 2017, **160**, 203–210.

51 H. Teng, J. Song, G. Xu, F. Gao and X. Luo, *Electrochim. Acta*, 2020, **355**, 136772.

52 M. K. Singh, A. K. Gupta, S. Krishnan, N. Guha, S. Marimuthu and D. K. Rai, *J. Energy Storage*, 2021, **43**, 103301.

53 X. Li, Y. Ma, P. Shen, C. Zhang, M. Cao, S. Xiao, J. Yan, S. Luo and Y. Gao, *Adv. Mater. Technol.*, 2020, **5**, 2000272.

54 K. L. Van Aken, M. Beidaghi and Y. Gogotsi, *Angew. Chem., Int. Ed.*, 2015, **127**, 4888–4891.

12598 | *J. Mater. Chem. C*, 2023, **11**, 12590–12598

This journal is © The Royal Society of Chemistry 2023